

INVESTIGATION OF THE ELECTRONIC PROPERTIES OF CARBON AND III-V NANOTUBES

Sam Azadi

A Thesis submitted for the degree of Doctor of Philosophy

Physics Department

University of Razi

March 2009

Abstract

The presence of defects such as impurities and structural defects (vacancies and Stone-Wale defects) particularly affect the electronic properties of nanotubes. Considering various potential applications of nanotubes (e.g. electrical circuits, gas sensors and transistors), we decided to investigate the electronic properties of pure and defected nanotubes (NTs). To this end, *ab initio* calculations usually are the best, specially density functional theory (DFT) based methods. In this regard, various kinds of NTs such as Single-walled (SW) and double-walled (DW) carbon nanotubes (CNT), boron nitride nanotubes (BNNT) and gallium nitride nanotubes (GaNNT) were analyzed.

Boron nitride semiconducting zigzag SWCNT, $B_{cb}N_{cn}C_{1-cb-cn}$, as a potential candidate for making nanoelectronic devices was examined. In contrast to the previous DFT calculations, wherein just one boron and nitrogen doping configuration have been considered, here for the average over all possible configurations, density of states (DOS) was calculated in terms of boron and nitrogen concentrations. It was shown that semiconducting average gap, E_g , could be controlled by doping nitrogen and boron. But in contrast to many-body techniques where gap edge in the average DOS is sharp, the gap edge is smeared and impurity states appear in the SWCNT semiconducting gap. For each boron and nitrogen concentrations, also, exact magnitude of the energy gap, E_g , was calculated.

Furthermore, Density functional theory (DFT) calculations of the Stone-Wales defected (S-WD) single-walled carbon nanotube (CNT) (10,0) were carried out to understand the effect of S-WD orientations on the electronic properties of CNT. We have considered the influence of supercell approximation on the defect formation energy and the electronic properties of both circumferential and axial S-W

defects in CNT. We found that the probability of S-WD orientation depends on the defect concentration. Density of states of defected CNTs calculations have been applied to indicate the effect of S-WD concentration on the semiconducting energy gap. Utilizing local density of states investigation, also, we explained the reasons of foreign atoms and molecules adsorption on S-WDs .

All BN nanotubes are semiconductor nanostructures regardless of diameter or chirality, in contrast to the carbon nanotubes that have both metallic and semi-conducting features. In this case, the electronic properties of defected BNNTs for spin-up and spin-down electrons were explored. We have looked into two types of defects, vacancy and substitution of carbon and oxygen by boron or nitrogen. The formation energy calculation reveals that for both vacancies defected zigzag and armchair BNNTs, the probability of the nitrogen vacancy case is higher than that of the boron one. Also in the carbon doping process of BNNTs, the substitution of boron by carbon is more possible with respect to nitrogen by carbon. In the oxygen doping substitution process, substitution of boron by oxygen is less favorable than nitrogen by oxygen. For the higher-probability cases the spin-up and spin-down band structures show different features. For the first and second cases, the spin-up band structure shows a n-type semiconductor, while the spin-down band structure illustrates a wide band gap semiconductor. But for the oxygen-doped BNNTs case, the spin-up band structure shows a wide band gap semiconductor, while the spin-down band structure illustrates a n-type semiconductor. All defected BNNTs have a $1.0 \mu_B$ total magnetic moment.

Like BNNTs, GaNNTs, another wide band gap nanostructures, are of interest. Structure and electronic properties of GaN nanotubes (GaNNTs) were studied in our work. The optimized structures (bond-lengths and angles between them) of zigzag GaNNTs ($n, 0$) and armchair GaNNTs (n, n) ($4 < n < 11$) were calculated by full optimization. The difference between nitrogen ring diameter and gallium ring diameter (buckling distance) and semiconducting energy gap in term of diameter for zigzag and armchair GaNNTs have also been calculated. We observed that buckling distance decreases by increasing nanotube diameter. Furthermore, we have examined the effects of nitrogen and gallium vacancies on structure and

electronic properties of zigzag GaNNT (5, 0) using spin dependent density functional theory. By calculating the formation energy, we determined that N vacancy in GaNNT (5, 0) is more favorable than Ga vacancy. The nitrogen vacancy in zigzag GaNNT induces a $1.0 \mu_B$ magnetization and makes a polarized structure. We realized that in polarized GaNNT a flat band near the Fermi energy splits to occupied spin up and unoccupied spin down levels.

Finally, the electronic properties of DWCNTs were investigated. The DWCNTs were separated into four categories wherein the innerouter nanotubes are metalmetal, metalsemiconductor, semiconductormetal and semiconductorsemiconductor single-wall nanotubes. The band structure of DWCNTs, the local density of states of the inner and outer nanotubes, and the total density of states were calculated. We obtained that for the metalmetal DWCNTs, the inner and outer nanotubes remain metallic for different distances between the walls, while for the metalsemiconductor DWCNTs, decreasing the distance between the walls leads to a phase transition in which both nanotubes become metallic. In the case of semiconductormetal DWCNTs, it is found that at some distance the inner wall becomes metallic, while the outer wall becomes a semiconductor, and if the distance is decreased, both walls become metallic. Finally, in the semiconductorsemiconductor DWCNTs, if the two walls are far from each other, then the whole DWCNT and both walls remain semiconducting. By decreasing the wall distance, first the inner, and then the outer, nanotube becomes metallic.

Acknowledgements

This thesis has been prepared in the Physics department of Razi university under Prof. Rostam Moradian supervision during the years 2006-2009. I am grateful to my supervisor, Prof. Rostam Moradian, since his passion and devotion to physics are contagious and his intuition has significantly inspired my research activity. One of his most striking qualities is the desire to deeply interact with his students, explain them all his thoughts, and take care of their ideas. Even in the busiest days, the door of his office is always open to receive whoever wants to speak to him. Finally, I would like to thanks a lot my parents for support.

February 2009,

Sam Azadi

List of Figures

1.1	High-resolution transmission electron microscopy pictures of a multiwall carbon nanotube (left) and a bundle of single-wall nanotubes(right), illustrating two different possible geometries for nanotubes.	3
1.2	Graphene honeycomb network with lattice vectors \mathbf{a}_1 and \mathbf{a}_2 . The chiral vector $\mathbf{c}_h = 5\mathbf{a}_1 + 3\mathbf{a}_2$ represents a possible wrapping of the two-dimensional graphene sheet into a tubular form. The direction perpendicular to \mathbf{C}_h is the tube axis. The chiral angle θ is defined by the \mathbf{C}_h vector and the \mathbf{a}_1 zigzag direction of the graphene lattice. In the present example, a (5,3) nanotube is under construction and the resulting tube is illustrated on the right.	4
1.3	Atomic structures of (12,0) zigzag, (6,6) armchair, and (6,4) chiral nanotubes.	5
1.4	The σ bonds in the carbon hexagonal network connect the carbon atoms and are responsible for the binding energy and the elastic properties of the graphene sheet (left). The π bonds are perpendicular to the surface of the sheet. The corresponding bonding and antibonding σ bands are separated by a large energy gap (right), while the bonding and antibonding π states lie in the vicinity of the Fermi level (E_F). [1]	8

1.5	Electronic properties of graphene. (a) Electronic band structure of graphene. The bonding σ and antibonding σ^* bands are separated by a large energy gap. The bonding π (last valence) band and antibonding π^* (first conduction) bands cross at the K points of the Brillouin zone. The Fermi energy is set to zero, and ϕ indicates the work function. Above the vacuum level (dotted horizontal line), the states of the continuum are difficult to describe and merge with the σ^* bands. (b),(d) π state at K and (c),(e) σ state at Γ , seen from above and from the side of the graphene plane. Note that the π function cancels on a hexagonal sublattice due to the $\exp(i\mathbf{K} \cdot \mathbf{r})$ phase factor. The π (σ) state is odd (even) with respect to the graphene plane reflection.	8
1.6	Brillouin zone and reciprocal space. (a) Basis vectors in the hexagonal lattice of graphene. (b) Brillouin zone. The corresponding reciprocal basis vectors read $\mathbf{b}_1 = b(1/2, \sqrt{3}/2)$ and $\mathbf{b}_2 = b(1/2, -\sqrt{3}/2)$, with $b = 4\pi/a\sqrt{3}$	9
1.7	The structures of BN compound. (a),(b) α BN, Planar hexagonal structure. (c) β BN, sphalerite structure and (d) wurtzite structure.	11
1.8	Structure of parent materials. (a) Graphite, $a = 2.456\text{\AA}$ and $c = 6.696\text{\AA}$ and (b) Boron nitride, $a = 2.504\text{\AA}$ and $c = 6.661\text{\AA}$	12
1.9	Band structures of graphene and a hexagonal BN sheet.	13
3.1	Density of states of: (a) a (10,0) zigzag single wall carbon nanotube. (b) where one of carbon atoms are substituted by a nitrogen atom in super-cell which included 120 carbon atoms (0.83 percent nitrogen doping). (c) where one of carbon atoms are substituted by a boron atom (0.83 percent boron doping).	45

- 3.2 (a) Density of states of a doped (10,0) zigzag single wall carbon nanotube by boron and nitrogen where boron concentration is fixed at $cb = 0.0005$ and nitrogen concentration is varied as $cn = 0.0005$ and $cn = 0.0025$. By increasing nitrogen concentration to $cn = 0.0025$, magnitude of both semiconducting gaps are decreased from $E_{g1} = 0.217\text{ev}$ and $E_{g2} = 0.054\text{ev}$ to $E_{g1} = 0.051\text{ev}$ and $E_{g2} = 0.0\text{ev}$ respectively. (b) Magnified semiconducting gap region of Fig.3.2(a). 46
- 3.3 illustrate filling semiconducting gaps by nitrogen states as a function of nitrogen concentrations where magnitude of gaps are $E_{g1} = 0.245\text{ev}$, $E_{g2} = 0.054\text{ev}$; $E_{g1} = 0.163\text{ev}$, $E_{g2} = 0.0\text{ev}$ and $E_{g1} = 0.109\text{ev}$, $E_{g2} = 0.0\text{ev}$ for nitrogen concentrations $cn = 0.0005$, $cn = 0.001$ and $cn = 0.0025$ respectively. 47
- 3.4 (a)Average density of states of a (10,0) SWCNT at a fixed nitrogen concentration, $cn = 0.0005$, for two different boron concentrations $cb = 0.0005$ and $cb = 0.0025$, magnitude of semiconducting gaps are decreased from $E_{g1} = 0.217\text{ev}$, $E_{g2} = 0.054\text{ev}$ to $E_{g1} = 0.027\text{ev}$, $E_{g2} = 0.0\text{ev}$ respectively. (b) Magnified gaps regions of Fig.3.2(a). Magnitude of gap is decreased by increasing boron concentration. 48
- 3.5 Magnified gaps regions in the averaged density of states at fixed nitrogen concentration $cn = 0.0002$ for various boron concentrations $cb = 0.0008$, $cb = 0.00012$ and $cb = 0.0016$. The semiconducting gaps are $E_{g1} = 0.217\text{ev}$, $E_{g2} = 0.054\text{ev}$; $E_{g1} = 0.161\text{ev}$, $E_{g2} = 0.0\text{ev}$ and $E_{g1} = 0.124\text{ev}$, $E_{g2} = 0.0\text{ev}$ respectively. By increasing boron concentration more impurity states are appeared in the semiconducting gap. 48

3.6	Comparison of a doped SWCNT semiconducting gap for two cases $cb = 0.0005$, $cn = 0.0025$ and $cb = 0.0025$, $cn = 0.0005$. The semiconducting gap in the case of $cb = 0.0025$, $cn = 0.0005$ is $E_{g2} = 0.027ev$ and shifted to the higher energies with respect to the $cb = 0.0005$, $cn = 0.0025$ where is $E_{g2} = 0.051ev$	49
3.7	Three types of Stone-Wales defects in a single-walled carbon nanotube (10,0) super-cell which included 160 carbon atoms. (a),(c) circumferential Stone-Wales defects, (b) axial Stone-Wales defect.	52
3.8	Density of states of: (a) perfect (10,0) SWCNT, (b) circumferential S-W defected SWCNT at 1/120 concentration, (c) axial defected SWCNT at 1/120 concentration.	55
3.9	Density of states of a defected (10,0) SWCNT for type one and type two Stone-Wales defects at 1/120 concentration.	55
3.10	A comparison between (10,0) SWCNT density of states for perfect, type one and type two Stone-Wales defects, where defect concentration is 1/160.	56
3.11	An illustration of density of states of axial S-W defected SWCNT (10,0), with two different defect concentrations 1/120 and 1/200.	57
3.12	Local density of states at sites 9 and 12 (Fig.1) for axial S-WD at 1/160 concentration.	58
4.1	Electronic band structures of single-walled BNNTs, (a) (5,0) with direct energy gap $E_g = 1.877ev$ and (b) (5,5) with indirect energy gap $E_g = 4.154ev$	63

4.2	Calculated band structures of nitrogen vacancy defected zigzag and armchair BNNTs. (a) Band structure of (5,0) BNNT for spin down electrons, the energy gap is $E_g = 1.73\text{ev}$. (b) Band structure of (5,0) BNNT for spin up electrons, where it is a <i>n-type semiconductor</i> with energy gap $E_g = 0.24\text{ev}$. (c) Band structure of (5,5) BNNT for spin down electrons, the energy gap is $E_g = 3.61\text{ev}$. (d) Band structure of (5,5) BNNT for spin up electrons, where it is a <i>n-type semiconductor</i> with energy gap $E_g = 0.44\text{ev}$. Zero point shows the Fermi energy.	65
4.3	Calculated band structures of carbon doped (5,0) and (5,5) BNNTs. (a) (5,0) spin down electrons band structure, where the energy gap is $E_g = 1.79\text{ev}$. (b) (5,0) band structure of spin up electrons, where the energy gap is $E_g = 0.77\text{ev}$. (c) (5,5) band structure for spin down electrons, where the energy gap is $E_g = 3.91\text{ev}$. (d) band structure of (5,5) for spin up electrons, where the energy gap is $E_g = 0.85\text{ev}$. Zero point shows the Fermi energy.	66
4.4	Calculated band structures of oxygen doped zigzag and armchair BNNTs (5,0) and (5,5). (a) (5,0) spin down electrons band structure, where the energy gap is $E_g = 0.31\text{ev}$, (b) (5,0) spin up electrons band structure, where the energy gap is $E_g = 2.12\text{ev}$, (c) (5,5) spin down electrons band structure, where the energy gap is $E_g = 0.11\text{ev}$ and (d) (5,5) spin up electrons band structure, where the energy gap is $E_g = 3.93\text{ev}$. Zero point shows the Fermi energy.	69
4.5	The optimized structure of (a) (5,0), (b) (10,0) GaNNTs.	75
4.6	Buckling distance for zigzag and armchair gallium nitride nanotubes. By diameter increasing the buckling distance reduces. . .	76
4.7	The band structures of zigzag (a) (5,0), (b) (7,0) and (c) (10,0) GaNNTs. By increasing the nanotube diameter the direct energy gap increases.	77

4.8	The band structures of armchair (a) (6,6), (b) (7,7) and (c) (8,8) GaNNTs. By increasing the nanotube diameter the indirect energy gap increases.	77
4.9	The energy gaps in terms of radius for zigzag and armchair GaNNTs. The energy gap increases by increasing nanotube radius. . .	78
4.10	The optimized structure of defected GaNNTs with nitrogen vacancy: GaNNT (5,0) where the bond lengths are $d_{1-2} = 1.96\text{\AA}$, $d_{1-3} = 2.52\text{\AA}$, $d_{4-5} = 1.95\text{\AA}$ and $d_{4-6} = 1.95\text{\AA}$	78
4.11	The band structures of GaNNT (5,0) with a nitrogen vacancy for (a) spin up electrons and (b) spin down electrons.	79
5.1	The band structure and density of states of a (8,8)@(12,12) double-wall carbon nanotube. The results show that the whole double wall, and also inner and outer walls are metallic.	87
5.2	The band structures of (6,0)@(10,0), (6,0)@(14,0) and (6,0)@(20,0) double-wall carbon nanotubes, where initially the separate inner SWCNT is metallic, while the outer SWCNT is a semiconductor. The band structure shows that the whole double-wall structure is metallic.	88
5.3	The density of states for individual SWCNTs (6,0)@(10,0) and (6,0)@(14,0) and (6,0)@(20,0) when they are parts of the DWCNTs. The results show that the separate SWCNTs in the (6,0)@(10,0) DWCNT and (6,0)@(14,0) DWCNT are metallic, while in the (6,0)@(20,0) DWCNT, the inner SWCNT remains metallic and the outer SWCNT remains semiconductor.	89
5.4	The band structures of (8,0)@(21,0), (10,0)@(21,0) and (14,0)@(21,0) DWCNTs where their initial SWCNTs semiconducting gaps are overlapped. By decreasing distance between layers, a semiconductor to metal phase transition takes place.	90
5.5	The densities of states of (8,0)@(21,0), (10,0)@(21,0) and (14,0)@(21,0).	

5.6	The inner wall and outer wall local densities of states for (8,0)@(21,0), (10,0)@(21,0) and (14,0)@(21,0) DWCNTs. For (8,0)@(21,0) inner wall is metallic while the outer wall is a semiconductor, where they are interchanged to metallic-semiconductor respectively. By increasing the inner wall radius, interactions between walls leads to a metal-to-semiconductor phase transition for inner wall.	92
5.7	The band structures of (8,0)@(20,0), (10,0)@(20,0) and (14,0)@(20,0) DWCNTs where their initial SWCNTs semiconducting gaps are overlapped. By decreasing distance between layers, a semiconductor-to-metal phase transition takes place.	93
5.8	The densities of states of (8,0)@(20,0), (10,0)@(20,0) and (14,0)@(20,0) DWCNTs. The semiconducting gap of initial SWCNTs of (8,0)@(20,0) are overlapped and the walls are far from each others, hence (8,0)@(20,0) is a semiconductor. Although semiconducting gap of initial SWCNTs of (10,0)@(20,0) and (14,0)@(20,0) are overlapped but interaction between walls leads to a semiconductor-to-metal phase transition.	94
5.9	The local density of states at a carbon atom position on the inner and outer walls of (8,0)@(20,0), (10,0)@(20,0) and (14,0)@(20,0) DWCNTs. In this case we found that, by decreasing the inter-wall distance, the interaction between walls could lead to a semiconductor-to-metal transition for both walls.	95

List of Tables

3.1	Formation energies of two types SW defect (S-WD) on SWCNT (10,0)	54
4.1	Calculated lattice constant in the z-direction, $c = 3 \times (\text{bond} - \text{length})$, and binding energy for $(n,0)$ ($n = 5 - 10$) zigzag GaN nanotubes.	80
4.2	Calculated lattice constant in the z-direction, $c = \sqrt{3} \times (\text{bond} - \text{length})$, and binding energy for (n,n) ($n = 5 - 10$) armchair GaN nanotubes.	81
4.3	Optimized bond-lengths of zigzag and armchair gallium nitride nanotubes.	82
4.4	Optimized angles between bond-lengths of zigzag and armchair gallium nitride nanotubes.	82

Contents

1	Introduction to Nanostructures	1
1.1	Introduction	2
1.2	Carbon Nanotubes	3
1.2.1	Structure of carbon nanotubes	3
1.2.2	Electronic properties of carbon nanotubes	7
1.3	III-V nanostructures	10
1.3.1	Structure of boron nitride compounds	10
1.3.2	Electronic properties of boron nitride nanotubes	11
2	Density Functional Theory Formalism	14
2.1	Introduction	15
2.2	Density Functional Theory: physical picture	16
2.2.1	Density functional formalism and derivation of the Kohn–Sham equations	19
2.3	The local density approximation	23
2.4	Exchange and correlation: a closer look	26
2.4.1	The adiabatic theorem and the normalisation conditions	26
2.4.2	The generalized gradient approximation	31
2.4.3	Exact exchange	31
2.5	Band structure methods and basis functions	32
2.5.1	Augmented plane wave methods	34
2.5.2	The linearised (LAPW) method	37
2.6	WIEN2k	41

3	Electronic Properties of Defected CNTs	42
3.1	Boron and nitrogen doped single-walled carbon nanotube	43
3.1.1	Introduction	43
3.1.2	Calculation method	44
3.1.3	Results and discussion	46
3.2	The effect of Stone-wales defect orientations on the electronic properties of single-walled carbon nanotubes	49
3.2.1	Introduction	49
3.2.2	Computational method	50
3.2.3	S-W defect formation energy	51
3.2.4	Electronic density of states	54
4	Magnetism in III-V Nanotubes	59
4.1	Magnetism in defected single-walled boron nitride nanotubes . . .	60
4.1.1	Introduction	60
4.1.2	Computational method	61
4.1.3	Results and discussion	62
4.2	Structure and electronic properties of native and defected gallium nitride nanotubes	70
4.2.1	Introduction	70
4.2.2	Computational Method	72
4.2.3	Results and Discussion	74
5	Inter-layer Interaction in DWCNTs	83
5.1	Introduction	84
5.2	Computational details and results	85

Chapter 1

Introduction to Nanostructures

1.1 Introduction

Since carbon nanotubes discovery in 1991, nanotubes have generated huge activity in most areas of science and engineering due to their unprecedented physical and chemical properties. No previous material has displayed the combination of superlative mechanical, thermal and electronic properties attributed to them. These properties make nanotubes ideal, not only for a wide range of applications¹ but as a test bed for fundamental science. The diverse fields, where in nanotubes are intensely studied and considered to have a huge potential application in all sorts of nanoscale devices, nanostructured materials or instrumentations containing nanoscale components, include computational and experimental nanoscience, theoretical and applied nanotechnology and molecular engineering, theoretical, computational and experimental condensed matter physics and chemistry, and many other fields.

The physics of nanotubes is connected with the exciting fields of computational nano-science, computational nano-technology and computational condensed matter physics. The bases of these fields are numerical modeling and computer-based simulation, to compute the physical properties of nano structures, and nano-scale processes. These new fields of research allows us to exercise a complete control over the structure and functioning of physical matter at the atomistic and molecular scales. Computational nano-scale modelling offers an invaluable tool for the design, fabrication, and quality control of devices and components, and helps clarify the energetics and dynamics of the atoms participating in such structures and the conditions for the final stability of such structures [2].

Computational modeling of properties of nanotubes is based either on the use of methods rooted in the many-body theories of quantum mechanics, such as the density functional theory (DFT) of atoms and molecules, or on the use of methods

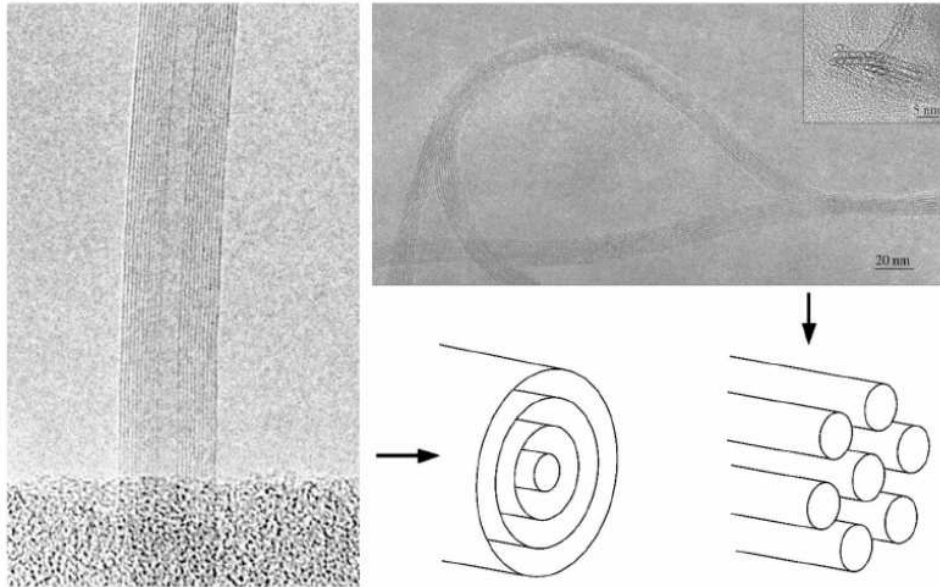


Figure 1.1: High-resolution transmission electron microscopy pictures of a multiwall carbon nanotube (left) and a bundle of single-wall nanotubes(right), illustrating two different possible geometries for nanotubes.

rooted in advanced classical statistical mechanics, such as the molecular dynamics (MD) simulation method. The quantum-mechanical approach allows for an *ab initio*, or first principles, study of nanoscale systems composed of several tens to, at most, several hundreds atoms, with current computational platforms. To be more familiar with different computational techniques in nanoscience, one of the best reference is Ref. [3].

1.2 Carbon Nanotubes

1.2.1 Structure of carbon nanotubes

Carbon nanotubes were discovered and first characterized in 1991 by Iijima from NEC laboratories (Japan) [4]. The first nanotubes discovered were made of several concentric cylindrical-like shells regularly spaced by an amount of about 3.4\AA as in conventional graphite materials (Fig. 1.2.1, left). These multiwall nanotubes (MWNTs) were first synthesized with diameters ranging from a few nanometers to several hundred nanometers for the inner and outer shells, respectively.

Shortly after the discovery of multiwall carbon nanotubes, single-wall carbon

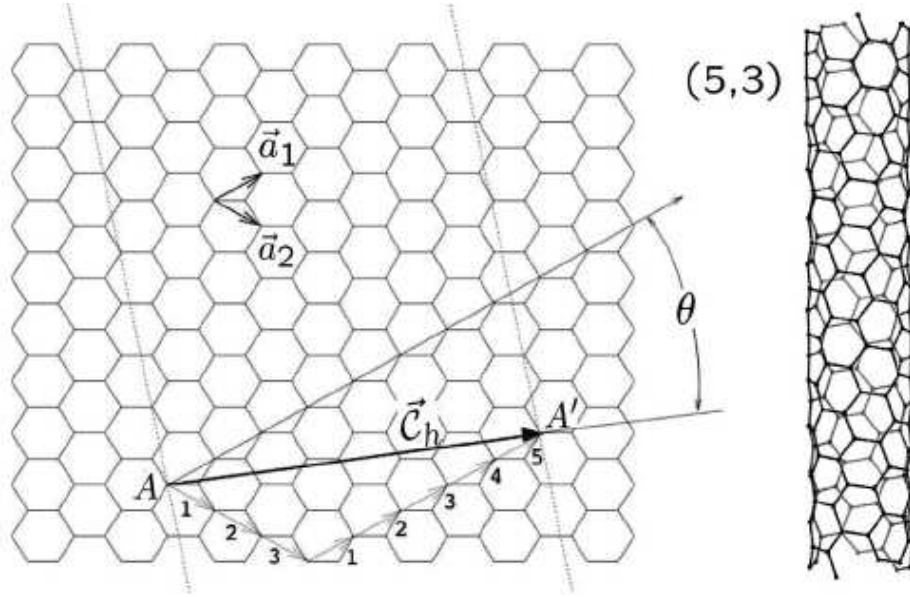


Figure 1.2: Graphene honeycomb network with lattice vectors \mathbf{a}_1 and \mathbf{a}_2 . The chiral vector $\mathbf{c}_h = 5\mathbf{a}_1 + 3\mathbf{a}_2$ represents a possible wrapping of the two-dimensional graphene sheet into a tubular form. The direction perpendicular to \mathbf{C}_h is the tube axis. The chiral angle θ is defined by the \mathbf{C}_h vector and the \mathbf{a}_1 zigzag direction of the graphene lattice. In the present example, a (5,3) nanotube is under construction and the resulting tube is illustrated on the right.

nanotubes (SWNTs) were synthesized in abundance using arc-discharge methods with transition-metal catalysts [5, 6]. A carbon naotube made of a single graphite layer (the graphene sheet) rolled up into a hollow cylinder is called a single-wall nanotube. These tubes have quite small and uniform diameter, on the order of $1nm = 10^{-9}m$. Because the microscopic structure of SWNTs is closely related to that of graphene, the tubes are usually labeled in terms of the graphene lattice vectors. As illustrated in Fig. 1.2.1 a single-wall carbon nanotube is geometrically obtained by rolling up a single graphene strip [7]. Its structure can be specified or indexed by its circumferential vector (\mathbf{C}_h), as defined by the chiral vector (AA' in Fig. 1.2.1) which connects two crystallographically equivalent sites (A and A') on a graphene sheet. In this way, a SWNT's geometry is completely specified by a pair of integers (n, m) denoting the relative position $\mathbf{C}_h = n\mathbf{a}_1 + m\mathbf{a}_2$ of the pair of atoms on a graphene strip which, when rolled onto each other, form a tube (\mathbf{a}_1 and \mathbf{a}_2 are unit vectors of the hexagonal honeycomb lattice).

This chiral vector \mathbf{C}_h defines the circumference of the tube. The diameter d_t of the nanotube can thus be estimated from

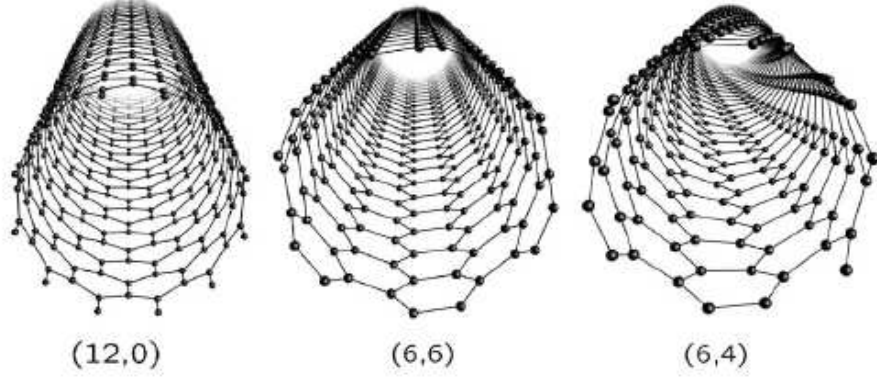


Figure 1.3: Atomic structures of (12,0) zigzag, (6,6) armchair, and (6,4) chiral nanotubes.

$$d_t = |\mathbf{C}_h|/\pi = \frac{a}{\pi} \sqrt{n^2 + nm + m^2}, \quad (1.1)$$

where a is the lattice constant of the honeycomb network: $a = \sqrt{3} \times a_{cc}$ ($a_{cc} \simeq 1.42\text{\AA}$, the C-C bond length). The chiral vector \mathbf{C}_h uniquely defines a particular (n,m) tube, as well as its chiral angle θ , which is the angle between \mathbf{C}_h and \mathbf{a}_1 (zigzag direction of the graphene sheet). The chiral angle θ can be calculated as:

$$\cos\theta = \frac{\mathbf{C}_h \cdot \mathbf{a}_1}{|\mathbf{C}_h| |\mathbf{a}_1|} = \frac{2n + m}{2\sqrt{n^2 + nm + m^2}}. \quad (1.2)$$

The value of θ is in the range $0 \leq |\theta| \leq 30^\circ$, because of the hexagonal symmetry of the graphene lattice. This chiral angle θ also denotes the tilt angle of the hexagonal with respect to the direction of the nanotube axis. Nanotubes of type $(n,0)$ ($\theta = 0^\circ$) are called zigzag tubes, because they exhibit a zigzag pattern along the circumference. Such tubes display carbon-carbon bonds parallel to the nanotube axis. Nanotubes of the type (n,n) ($\theta = 30^\circ$) are called armchair tubes, because they exhibit an armchair pattern along the circumference. Such tubes display carbon-carbon bonds perpendicular to the nanotube axis. Both zigzag and armchair nanotubes are chiral tubes, in contrast with general $(n,m \neq n \neq 0)$ chiral tubes (1.2.1).

The geometry of the graphene lattice and the chiral vector determine not only the diameter of the tube, but also the unit cell and its number of carbon atoms. The smallest graphene lattice vector \mathbf{T} perpendicular to \mathbf{C}_h defines the translational